Electronic Supporting Information

to

Phase transitions and optical properties of the trigonal perovskite $(CH_3NH_3)_2TeCl_6$

Yuhan Liu, Jeremy K. Cockcroft, Zizhen Chen, Michael A. Hayward, Paul F. Henry, Robin S. Perry, and Robert G. Palgrave

Table of Contents Page No.

Additional Experimental Details

1. Chemicals and synthesis

Tellurium oxide (TeO_2, 99.995%, Sigma-Aldrich), methylamine solution (CH_3NH_2, 40 wt. % in H_2O, Sigma-Aldrich), and hydrochloric acid (HCl, 37%, Fisher) were used as supplied. All reactions and manipulations were carried out in air.

First, 10ml 37% HCl was added to 0.798 g TeO_2. Separately, 10ml 37% HCl was cautiously added to ice cold 0.78 g CH_3NH_2 solution. In this way, clear solutions of $TeCl_4$ and MACl were obtained. Then these two solutions were mixed while stirring at 60 °C, resulting in a clear yellow solution. The solution was stirred for 30 minutes then slowly cooled down to room temperature over 5 h. In this way, hexagonal-shape single crystals suitable for diffraction studies were grown successfully.

2. Single-crystal X-ray diffraction (SXD)

All single crystal measurements were taken using the crystal shown in Fig. S1. Initially measurements were made with Cu Kα X-ray radiation, but these were subsequently repeated 2 days later with Mo Kα X-ray radiation. The results reported here are those obtained using an Agilent Oxford Diffraction SuperNova equipped with a microfocus Mo Kα X-ray source and an Atlas CCD detector. Full spheres of data were collected to 0.8 Å resolution using 1° scan frames in ω. Total collection time for each temperature was approximately 40 minutes. The Cryojet5® used for these measurements is the original prototype device developed by Oxford Instruments and the Pt-resistance sensor is located in the copper-block heat exchanger and not in the nozzle of the instrument close to the sample (in contrast to the CryojetHT® used in the PXRD experiments). Thus the temperatures quoted in these SXD experiments should be treated as nominal (despite stability to much better than 0.1 °C). The order of the measurements did not follow a simple high to low or low to high temperature sequence: the crystal was first measured at room temperature (295 K) and then cooled down to 160 K; subsequent measurements were carried out at 200 K, 90 K, 120 K, and 250 K, respectively.

SXD data were processed with CrysAlisPro 1.171.41.93a. The structure was solved with SHELXT[1] and refined with SHELXL[2] within the Olex2 software suite[3]. In common with many crystals exhibiting trigonal symmetry, the crystal was twinned with respect to the threefold axis with a twin parameter BASF approximately equal to 0.8. The H atoms of the $–CH_3$ and $–NH_3$ groups were constrained with respect to geometry but not with respect to orientation within the crystal. Octahedral rotation angles and interatomic distances within the crystal structure were calculated using the Mercury[4] software from CCDC. Crystal structure figures were drawn using either CrystalMaker[5] or Mercury[4]. Given that 2θ resolution is lower in SXD than in PXRD resulting in less precise lattice parameters in SXD, lattice parameter used in the structure calculation were taken from the VT-PXRD results.

3. Powder X-ray diffraction (PXRD)

A room temperature PXRD data set was obtained using a Stoe Stadi-P X-ray diffractometer equipped with a Mo tube set to 50 kV, 30 mA ($Kα_1$ with λ = 0.7093 Å), a primary beam monochromator, and Mythen

[1] G. M. Sheldrick, *Acta Crystallogr. Sect. A Found. Crystallogr.*, 2015, **71**, 3–8.
[2] G. M. Sheldrick, *Acta Crystallogr. Sect. C Struct. Chem.*, 2015, **71**, 3–8.
[3] O. V. Dolomanov, L. J. Bourhis, R. J. Gildea, J. A. K. Howard and H. Puschmann, *J. Appl. Crystallogr.*, 2009, **42**, 339–341.
[4] C. F. MacRae, I. Sovago, S. J. Cottrell, P. T. A. Galek, P. McCabe, E. Pidcock, M. Platings, G. P. Shields, J. S. Stevens, M. Towler and P. A. Wood, *J. Appl. Crystallogr.*, 2020, **53**, 226–235.
[5] *CrystalMaker®. CrystalMaker Software Ltd, Oxford, England (www.crystalmaker.com)*

detector. Measurements were made in thin-foil transmission mode with a 0.5° detector step for the 2θ range 2° to 40° counting at 10 s per step.

Variable temperature PXRD was obtained using a Stoe Stadi-P X-ray diffractometer equipped with a Cu tube set to 40 kV, 30 mA ($K\alpha_1$ λ = 1.5406 Å), a primary beam monochromator, and Mythen detector. Measurements were made in capillary mode with a 0.3 mm X-ray glass capillary, which was flame sealed. PXRD data were collected for the 2θ range 2° to 80° with a step size of 0.5° at 15 s per step. An Oxford Instruments CryojetHT was used to cool the sample to 120 K and then to heat it in increments of 20 K to 500 K with PXRD patterns obtained at each temperature. The lattice parameter of MA_2TeCl_6 at each temperature was determined by whole pattern least-squares fitting with GSAS II[6]. The results are listed in Table S1.

4. Neutron powder diffraction (NPD)

NPD can provide key information on light weight atoms and distinguish carbon and nitrogen inside the crystal structure due to their different scattering lengths (b_C = 6.646 fm; b_N = 9.36 fm). Time-of-flight NPD data were collected on MA_2TeCl_6 at room temperature using the General Materials Diffractometer (GEM) at the ISIS Muon and Neutron Spallation Source, UK. The sample was not deuterated (*i.e.* it contained 1H and not 2D), so the data has a higher background count than for a deuterated sample. Data was recorded on bank 4 of GEM with *d*-spacing range 0.2 to 3.7 Å.

Structure refinements were carried out using the GSAS II software suite[6], starting with the example structure of $MAPbI_3$, which had been previously reported.[7] Analysis of the NPD data was via GSAS II[6] and atomic positions from SXD data for MA_2TeCl_6 at RT (phase II) were used as basic for the structural model. Initial refinements were carried out without the MA^+ molecule, *i.e.* the crystal model only contained the $[TeCl_6]^{2-}$ octahedra, and a profile fit parameter R_{wp} = 1.81% was achieved.

The MA^+ molecule was then introduced into the calculation. To consider the spinning about C–N axis at RT, only one H site was placed on both end of C and N while the fractional occupancy was set as 0.5. Consequently, the bond lengths of C–N, C–H and N–H bonding were restrained as 1.4 Å, 1.1 Å and 1.0 Å; H–C–N and H–N–C angles were restrained as 109.54° to control the H atom positions; the distances between two H atoms on adjacent points of symmetry were restrained as 0.95 Å and 1.03 Å at N and C end respectively. Displacement parameters values for H atoms were constrained to be equal due to similar thermal motions. Profile parameters, atomic coordinates and atomic displacement parameters for Te and Cl were refined at first then the atomic coordinates and displacement parameters of MA^+ molecule were included. For the best fit, R_{wp} was 0.80% with a goodness of fit equal to 2.8. The NPD results are consistent with a model of the MA^+ molecule rotating around the C–N axis at room temperature.

5. Calculation of cation cavity

Several approaches were tried to describe the size of cation cavity. Initially, as the cavity is formed by 12 halogen atoms, the average distance between two adjacent halogen atoms $\overline{d}_{X-X}$ was calculated using CrystalMaker[5]. However, *R* values of different structures did not have an obvious variation as shown in Table S3 and Fig. S10(a). The distortion of the cavity was then taken into consideration. Inorganic cations and small organic A-site cations that behave as spherical, are usually surrounded by regular tetradecahedron cavities. However, for the larger organic cations which cannot be treated with a spherical model, the cavities may be distorted and the cations may have a hindered rotation inside the structure. Thus, the distance between halogen and the A-site cation, d_{A-X}, may better describe the cavity

[6] B. H. Toby and R. B. Von Dreele, *J. Appl. Crystallogr.*, 2013, **46**, 544–549.

[7] M. T. Weller, O. J. Weber, P. F. Henry, A. M. Di Pumpo and T. C. Hansen, *Chem. Commun.*, 2015, **51**, 4180–4183.

size. To simplify the model, the centre of mass of the A-site cation is used and the average distance $\overline{d}_{A-X}$ is easily calculated and applied in the radius ratio calculations. The results are shown in Fig. S10(b).

Calculations using both $\overline{d}_{X-X}$ and $\overline{d}_{A-X}$ do not make the $Fm\overline{3}m$ structure distinct from other structures, which might be because an average value loses the features of the distorted cavity. Therefore, the shortest distances d_{X-X} and d_{A-X}, which may better reflect the degree of cavity distortion, were used in the calculations. As shown in Fig. S10(c) and (d), a larger variation in R occurs using the shortest d_{A-X} which can better distinguish the $Fm\overline{3}m$ structure from the others.

Table S1 Lattice parameters of MA_2TeCl_6 obtained from VT-PXRD using GSAS II[6].

Temperature /K	*a*/Å	*b*/Å	*c*/Å	α/°	*β*/°	*γ*/°	volume/Å^3
120	12.5657(2)	12.5657(2)	14.2088(3)	90	90	120	1942.95(6)
140	12.5810(2)	12.5810(2)	14.2080(2)	90	90	120	1947.56(5)
160	12.5970(2)	12.5970(2)	14.2073(2)	90	90	120	1952.44(4)
180	12.6149(2)	12.6149(2)	14.2076(2)	90	90	120	1958.03(5)
200	12.6343(2)	12.6343(2)	14.2090(2)	90	90	120	1964.25(5)
220	7.3051(1)	7.3051(1)	7.1019(1)	90	90	120	328.21(1)
240	7.3179(1)	7.3179(1)	7.0984(1)	90	90	120	329.20(1)
260	7.3314(1)	7.3314(1)	7.0935(1)	90	90	120	330.19(1)
280	7.3450(1)	7.3450(1)	7.0876(1)	90	90	120	331.14(1)
300	7.3596(1)	7.3596(1)	7.0805(1)	90	90	120	332.13(1)
320	7.3746(1)	7.3746(1)	7.0718(1)	90	90	120	333.08(1)
340	7.3906(1)	7.3906(1)	7.0624(1)	90	90	120	334.07(1)
360	7.4069(2)	7.4069(2)	7.0519(1)	90	90	120	335.05(1)
380	7.4238(2)	7.4238(2)	7.0398(1)	90	90	120	336.01(1)
400	7.4413(2)	7.4413(2)	7.0278(1)	90	90	120	337.02(1)
420	7.4584(2)	7.4584(2)	7.0157(1)	90	90	120	337.98(1)
440	7.4757(2)	7.4757(2)	7.0037(2)	90	90	120	338.97(1)
460	7.4934(4)	7.4934(4)	6.9919(2)	90	90	120	340.00(3)
460	11.1952(6)	11.1952(6)	11.1952(6)	90	90	90	1403.12(2)
480	11.2112(2)	11.2112(2)	11.2112(2)	90	90	90	1409.16(7)
500	11.2266(2)	11.2266(2)	11.2266(2)	90	90	90	1414.96(7)

Table S2 Projected intermolecular distances and bond lengths (see Fig. S9) calculated using Mercury[4] from the atomic coordinates derived from the variable temperature SXD results. Given that the typical error of the projected lattice parameters is less than 0.002 Å, the error for all the projected distances and bond lengths will be less than 0.002 Å.

Temperature	*a*/Å	*c*/Å	Cl···Cl *a*/Å	Cl—Cl *a*/Å	Cl···Cl *c*/Å	Cl—Cl *c*/Å	N···Cl/Å	C···C/Å	C—N/Å
90 K	7.227	7.106	3.617	3.549	4.246	2.860	0.1650	1.646	1.468
120 K	7.243	7.089	3.630	3.547	4.235	2.853	0.1580	1.687	1.437
160 K	7.267	7.092	3.649	3.564	4.243	2.849	0.1490	1.682	1.433
200 K	7.283	7.095	3.665	3.581	4.251	2.844	0.1410	1.694	1.420
250 K	7.325	7.092	3.700	3.625	4.257	2.835	0.1400	1.713	1.411
295 K	7.357	7.081	3.730	3.627	4.248	2.833	0.1360	1.707	1.407

Table S3 Percentage interatomic distance changes, d/d_{90K}, derived from Table S2. The error for all the values will be less than 0.02%.

Temperature	*a*	*c*	Cl···Cl *a*	Cl—Cl *a*	Cl···Cl *c*	Cl—Cl *c*	N···Cl	C···C	C—N
90 K	100.0%	100.0%	100.0%	100.0%	100.0%	100.0%	100.0%	100.0%	100.0%
120 K	100.2%	99.8%	100.4%	99.9%	99.7%	99.8%	104.2%	102.5%	97.9%
160 K	100.6%	99.8%	100.9%	100.4%	99.9%	99.6%	109.7%	102.2%	97.6%
200 K	100.8%	99.8%	101.3%	100.9%	100.1%	99.4%	114.5%	102.9%	96.7%
250 K	101.4%	99.8%	102.3%	102.1%	100.3%	99.1%	115.2%	104.1%	96.1%
295 K	101.8%	99.6%	103.1%	102.2%	100.0%	99.1%	117.6%	103.7%	95.8%

Table S4 Cation radii (Å) and corresponding radius ratio R calculations.

Compound	r_A/Å	**R** average d_{X-X}	**R** shortest d_{X-X}	**R** average d_{A-X}	**R** shortest d_{A-X}	Structure
K_2TeI_6	1.64	0.83	0.88	0.86	1.19	Monoclinic (*P*2$_1$/*n*)
Rb_2TeI_6	1.72	0.97	0.92	0.90	1.03	Tetragonal (*P*4/*mnc*)
Cs_2TeI_6	1.88	0.89	0.97	0.97	0.97	Cubic (*Fm*$\bar{3}$*m*)
$(NH_4)_2TeI_6$	1.7	0.88	0.92	0.89	1.12	Monoclinic (*P*2$_1$/*n*)
$(CH_3NH_3)_2TeI_6$	2.38	1.17	1.21	1.17	1.17	Cubic (*Fm*$\bar{3}$*m*)
$((CH_3)_3NH)_2TeI_6$	3.04	1.20	1.54	1.21	1.56	Cubic (*Pa*$\bar{3}$)
K_2TeBr_6	1.64	0.88	0.90	0.89	1.17	Monoclinic (*P*2$_1$/*n*)
K_2TeBr_6	1.64	0.89	0.91	0.89	0.98	Tetragonal (*P*4/*mnc*)
K_2TeBr_6	1.64	0.89	0.92	0.89	0.89	Cubic (*Fm*$\bar{3}$*m*)
Rb_2TeBr_6	1.72	0.99	0.93	0.93	0.93	Cubic (*Fm*$\bar{3}$*m*)
Cs_2TeBr_6	1.88	0.93	1.01	0.99	0.99	Cubic (*Fm*$\bar{3}$*m*)
$(NH_4)_2TeBr_6$	1.7	0.93	0.93	0.93	0.93	Cubic (*Fm*$\bar{3}$*m*)
$(CH_3NH_3)_2TeBr_6$	2.38	1.14	1.27	1.14	1.14	Cubic (*Fm*$\bar{3}$*m*)
$((CH_3)_4N)_2TeBr_6$	3.01	1.09	1.64	1.08	1.24	Cubic (*Fd*$\bar{3}$*c*)
$((CH_3)_3NH)_2TeBr_6$	3.04	1.21	1.65	1.24	1.59	Cubic (*Pa*$\bar{3}$)
K_2TeCl_6	1.64	0.92	0.93	0.92	0.92	Monoclinic (*I*2/*m*)
Rb_2TeCl_6	1.72	1.00	0.98	0.95	0.95	Cubic (*Fm*$\bar{3}$*m*)
Cs_2TeCl_6	1.88	0.95	1.08	1.00	1.00	Cubic (*Fm*$\bar{3}$*m*)
$(NH_4)_2TeCl_6$	1.7	0.95	0.97	0.95	0.95	Cubic (*Fm*$\bar{3}$*m*)
$(CH_3NH_3)_2TeCl_6$	2.38	1.14	1.39	1.13	1.31	Trigonal (*P*$\bar{3}$1*c*)
$(CH_3NH_3)_2TeCl_6$	2.38	1.13	1.39	1.12	1.25	Trigonal (*P*$\bar{3}$*m*1)
$(CH_3NH_3)_2TeCl_6$	2.38	1.10	1.38	1.10	1.10	Cubic (*Fm*$\bar{3}$*m*)
$((CH_3)_2NH_2)_2TeCl_6$	2.96	1.21	1.78	1.24	1.56	Orthorhombic (*Pnnm*)
$((CH_3)_3NH)_2TeCl_6$	3.04	1.18	1.74	1.17	1.54	Cubic (*Pa*$\bar{3}$)
K_2SnCl_6	1.64	0.94	1.02	0.95	1.21	Monoclinic (*P*2$_1$/*n*)
K_2SnCl_6	1.64	0.95	1.07	0.95	1.01	Tetragonal (*P*4/*mnc*)
K_2SnCl_6	1.64	0.95	1.03	0.95	0.95	Cubic (*Fm*$\bar{3}$*m*)
Rb_2SnCl_6	1.72	0.91	1.06	0.97	0.97	Cubic (*Fm*$\bar{3}$*m*)
Cs_2SnCl_6	1.88	0.97	1.15	1.02	1.02	Cubic (*Fm*$\bar{3}$*m*)
$(NH_4)_2SnCl_6$	1.7	0.97	1.05	0.97	0.97	Cubic (*Fm*$\bar{3}$*m*)
$(N_2H_5)_2SnCl_6$	2.2	1.07	1.36	1.05	1.45	Orthorhombic (*Pnca*)
$(CH_3NH_3)_2SnCl_6$	2.38	1.14	1.50	1.13	1.30	Rhombohedral (*R*$\bar{3}$*m*)
$((CH_3)_2NH_2)_2SnCl_6$	2.96	1.25	1.90	1.25	1.63	Orthorhombic (*Pnnm*)
$(C_2H_5NH_3)_2SnCl_6$	2.99	1.25	1.90	1.21	1.48	Trigonal (*P*$\bar{3}$*m*1)
$((CH_3)_4N)_2SnCl_6$	3.01	1.09	1.87	1.07	1.21	Cubic (*Fd*$\bar{3}$*c*)
$((CH_3)_4N)_2SnCl_6$	3.01	1.08	1.88	1.06	1.06	Cubic (*Fm*$\bar{3}$*m*)

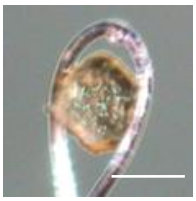

Fig. S1 Face view of the sample of MA_2TeCl_6 used in the SXD experiments showing the flat hexagonal shape. Scale bar is 200 µm.

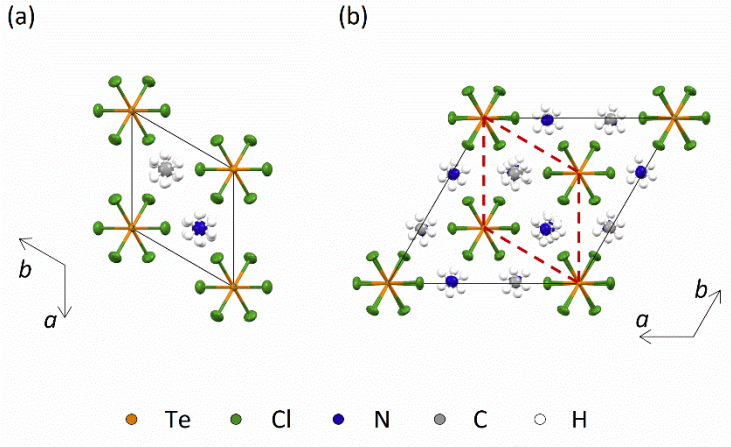

Fig. S2 MA_2TeCl_6 crystal structure seen along the *c*-axis (a) in phase II at 295 K (rotated 90°) and (b) in phase III at 200 K. The red dashed lines indicate phase III is related to phase II by a doubling of the unit along *c* and a $\sqrt{3}$ increase in *a*.

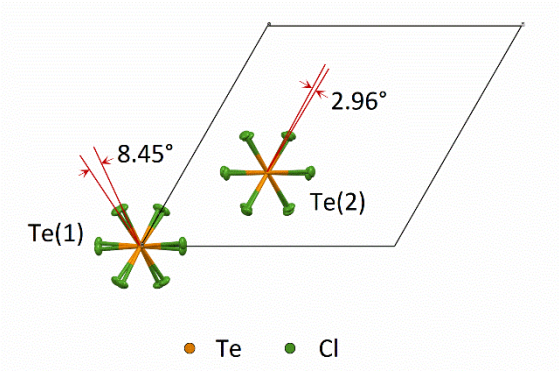

Fig. S3 MA_2TeCl_6 crystal structure seen along the *c*-axis illustrating the noticeable rotation of octahedra about the *c*-axis in phase III (90 K). The $[Te(1)Cl_6]^{2-}$ octahedra have a larger rotation angle compared to the $[Te(2)Cl_6]^{2-}$ octahedra. The rotation angle increases with decreasing temperature. Rotation angles are calculated with Mercury[4], which does not provide a calculated error value. Given that the internal bond angle Cl-Te-Cl has a typical error of 0.04° at 90 K, the error for the rotation angles will be around 0.1°.

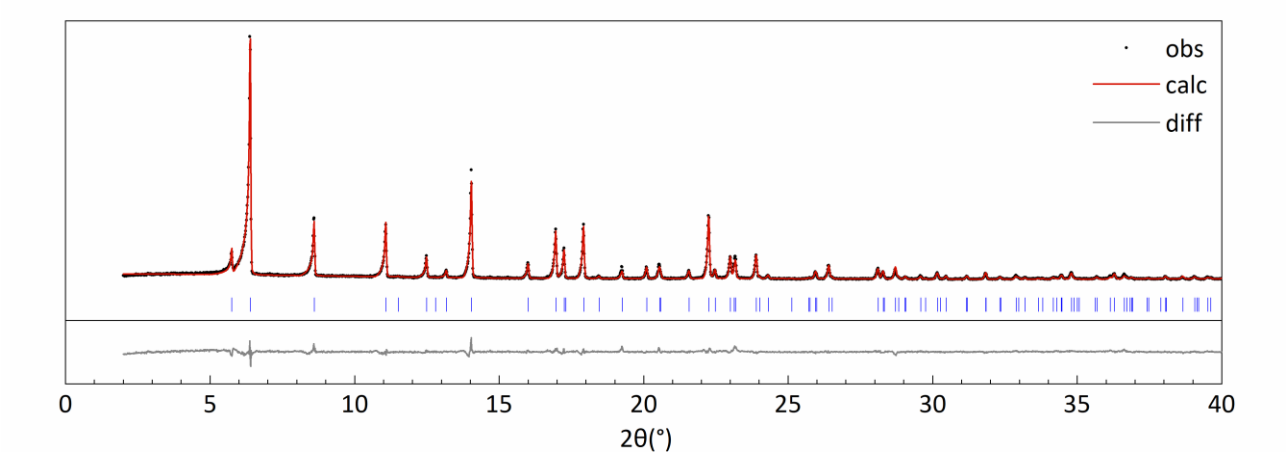

Fig. S4 Rietveld refinement of the room-temperature structure of MA_2TeCl_6 from PXRD data, collected with Mo radiation ($K\alpha_1$ with λ = 0.7093 Å). Observed data points are shown as black dots, the calculated PXRD pattern as a red line, and the difference curve is shown in grey. The calculated positions of the reflections are shown as vertical blue tick marks.

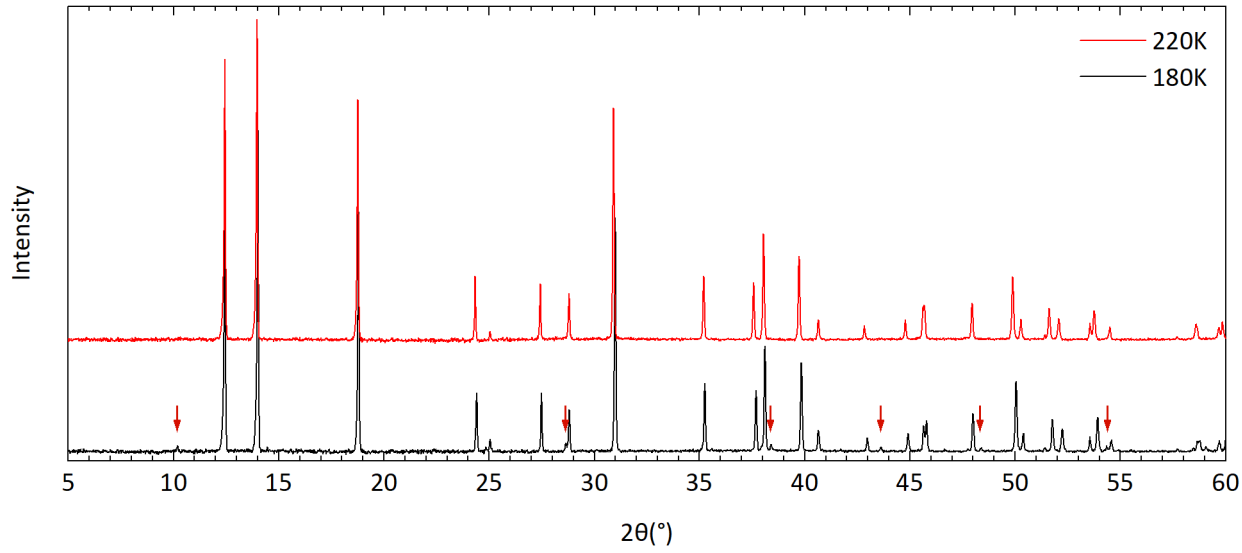

Fig. S5 Comparison of the PXRD patterns of MA_2TeCl_6 at 180 K (phase III) and 220 K (phase II), collected with Cu radiation ($K\alpha_1$ with λ = 1.5406 Å). Red arrows point out peaks that disappear on heating, which is consistent with a second-order phase transition.

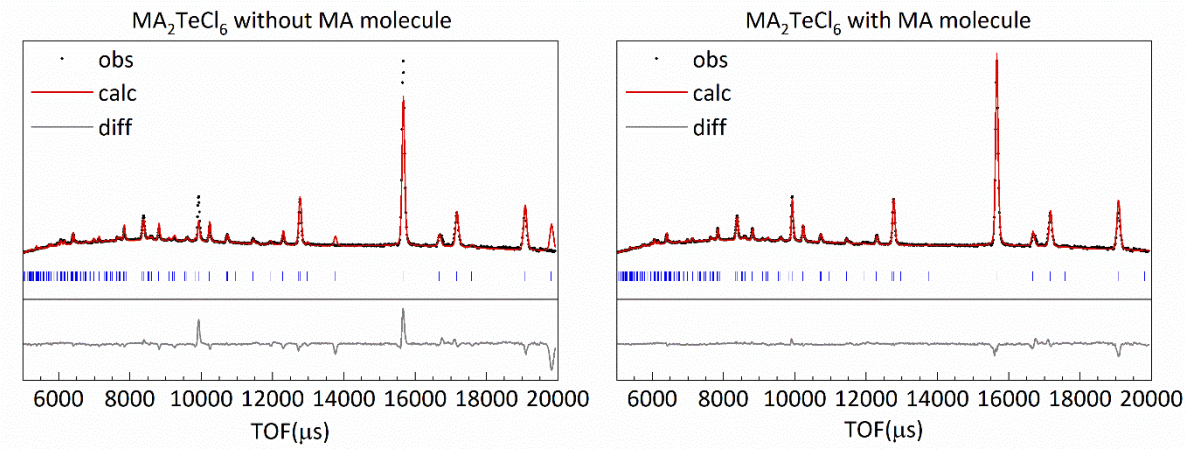

Fig. S6 Comparison of the fits obtained from Rietveld refinement of the crystal structure of MA_2TeCl_6 at room temperature to NPD data collected on GEM at ISIS, RAL, (left) without an MA^+ cation and (right) with an MA^+ cation included. The fit to the NPD data is clearly sensitive to the inclusion of MA^+ cation in the refinement as shown by the much better fit in the right-hand plot. Observed data points are shown as black dots, the calculated NPD pattern as a red line, and the difference curve is shown in grey. The calculated positions of the reflections are shown as vertical blue tick marks.

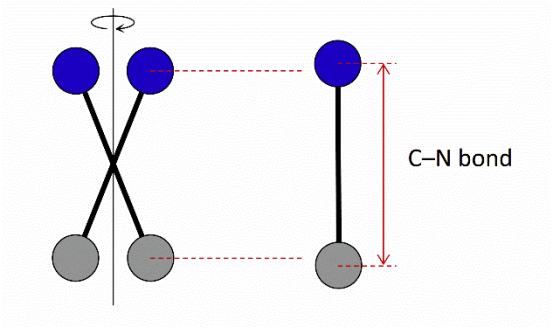

Fig. S7 Schematic showing off-axis rotation of the MA^+ cation in phase II producing a cone for the average position of the N and C atoms, leading to the shortened C–N bond length in our model. Blue represents N and grey represents C, red dashed lines indicate the apparent shortening of C–N bond.

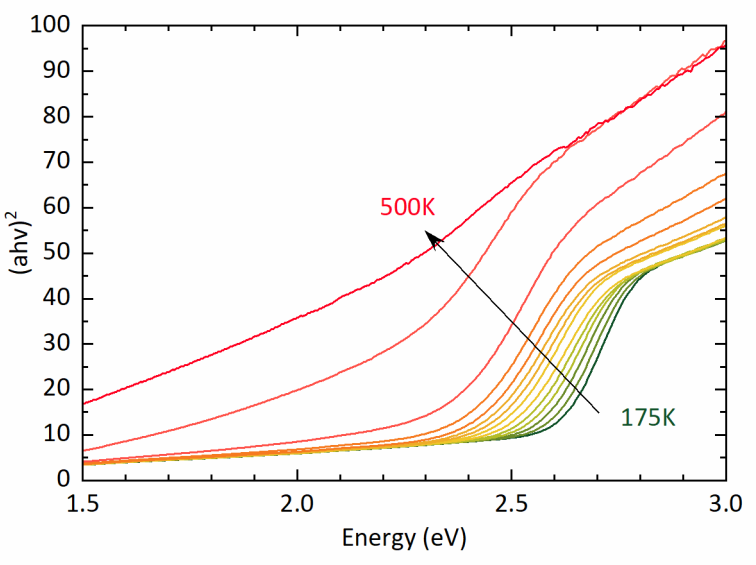

Fig. S8 Tauc plot derived from absorption spectra collected on a sample of MA_2TeCl_6 measured at 175 K to 500 K.

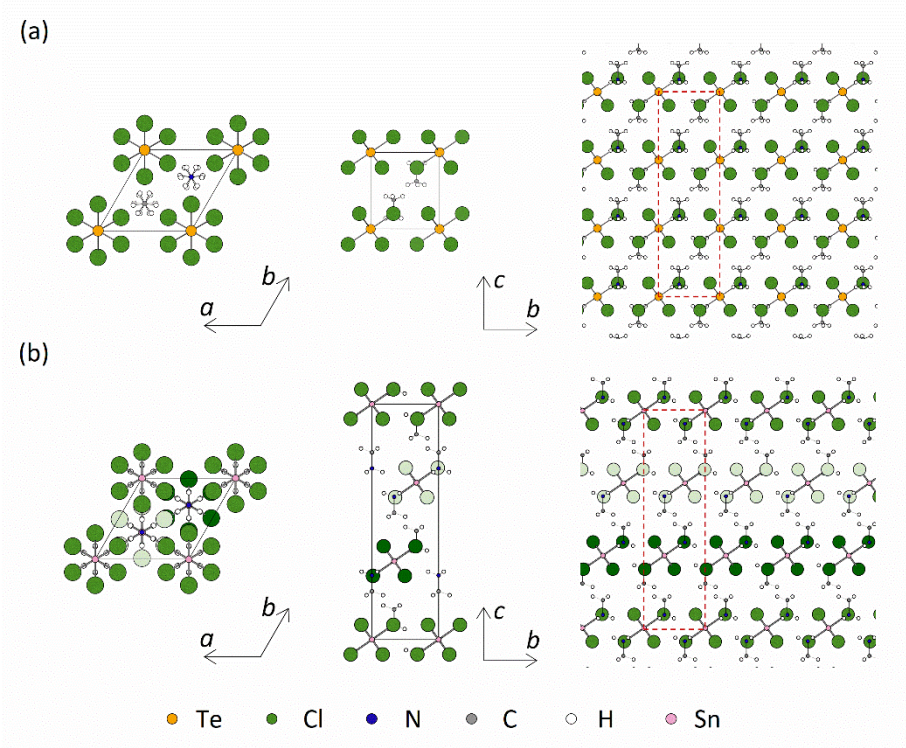

Fig. S9 Comparison of the crystal structures of (a) MA_2TeCl_6 and (b) MA_2SnCl_6 seen along the *c*-axis of the unit cell (left), down the *a*-axis (middle), and layers of octahedra for the two structures (right). The stacking of the layers is different between the two compounds: in MA_2TeCl_6, the $[TeCl_6]^{2-}$ anions lie directly above each other, whereas in MA_2SnCl_6 the layer at $z = ⅓$ is displaced relative to the layer at $z = 0$ by ⅔ and ⅓ in *a* and *b*, respectively. Different shades of green are used to represent Cl atoms belonging to different octahedra.

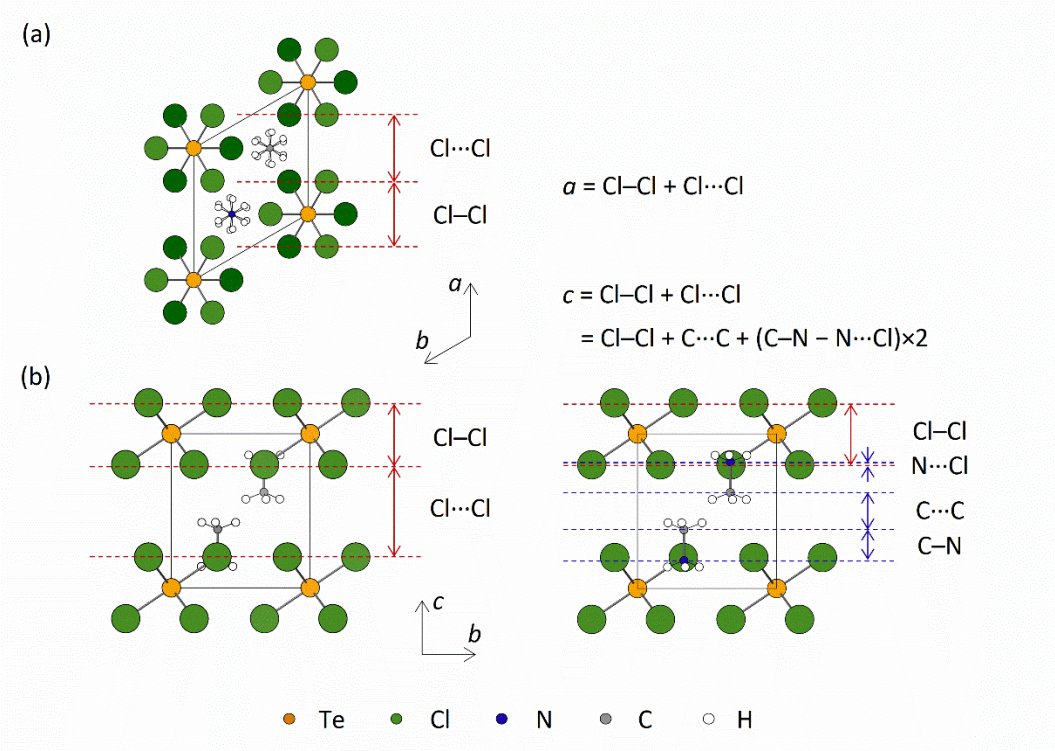

Fig. S10 Showing various distances as seen in projection for the crystal structure of MA_2TeCl_6 (a) viewed along *c* and (b) viewed along *a*. Cl–Cl and Cl···Cl represent the projection distances within octahedra and between octahedra, respectively. C···C, N···Cl, and C–N represent the projection distances between MA^+ cation layers, the overlapped distance between the layers of octahedra and MA^+ cations, and the C–N bond length with respect to the *c*-axis direction, respectively. Different shades of green in (a) are used to represent Cl atoms belonging to different layers.

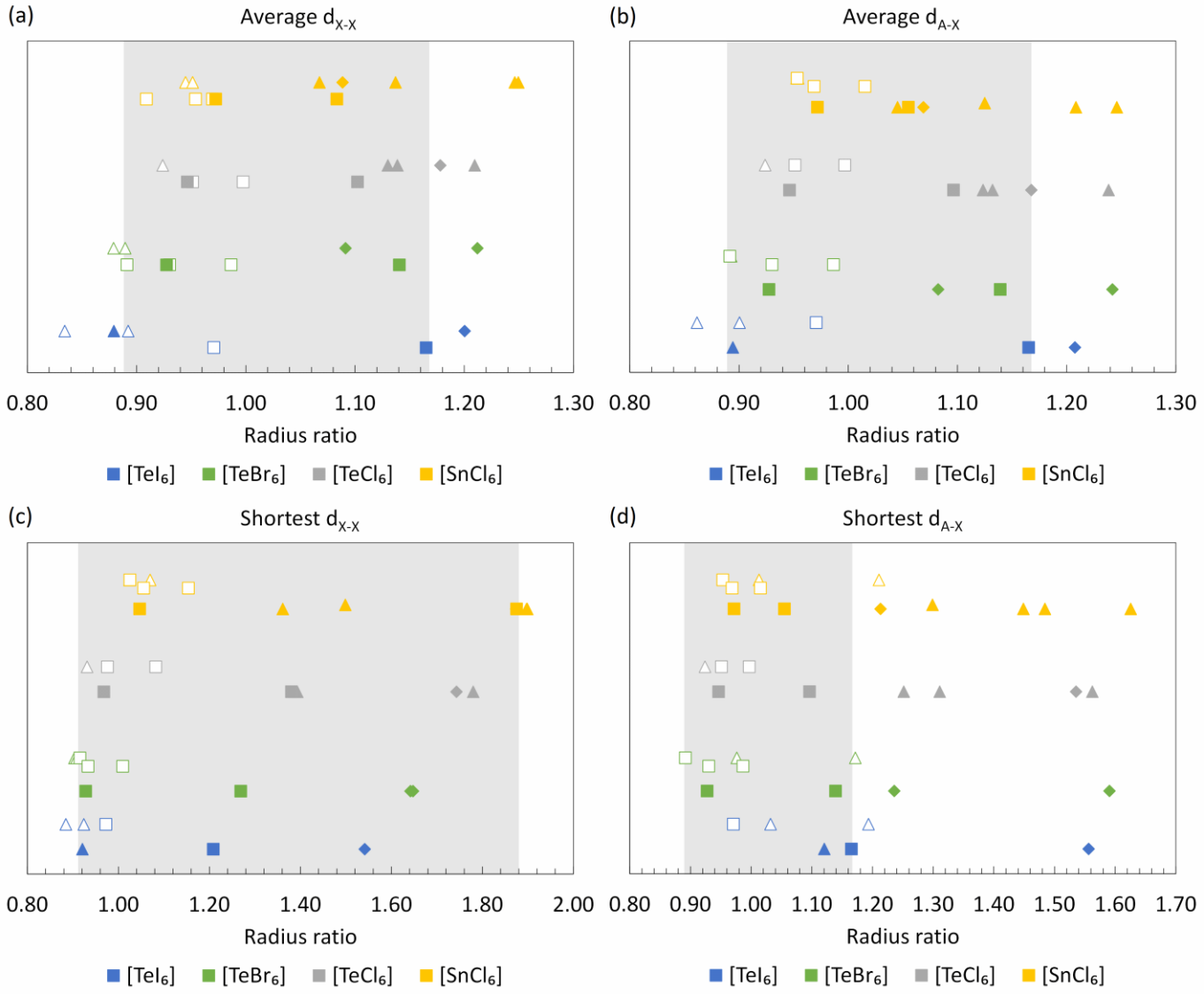

Fig. S11 Comparison of radius ratio calculations for A_2TeX_6 and A_2SnCl_6 compounds using (a) average d_{X-X}, (b) average d_{A-X}, (c) shortest d_{X-X},.and (d) shortest d_{A-X}, where the *Fm*$\bar{3}$*m* cubic structure range is picked out in grey. Square, diamond, and triangle symbols represent the *Fm*$\bar{3}$*m* cubic structure, other cubic structures, and non-cubic structures respectively; solid symbols represent organic cation structures and hollow symbols represent inorganic ones.